Food and Chemical Toxicology 126 (2019) 25–33

Contents lists available at ScienceDirect

Food and Chemical Toxicology

journal homepage: www.elsevier.com/locate/foodchemtox

Probiotic *Bacillus subtilis* CW14 reduces disruption of the epithelial barrier and toxicity of ochratoxin A to Caco-2 cells

Mengxue Peng[a], Jiawei Liu[a], Zhihong Liang[a,b,c,*]

[a] Beijing Advanced Innovation Center for Food Nutrition and Human Health, College of Food Science and Nutritional Engineering, China Agricultural University, Beijing, China
[b] The Supervision, Inspection and Testing Center of Genetically Modified Organisms, Ministry of Agriculture, Beijing, China
[c] Beijing Laboratory for Food Quality and Safety, College of Food Science and Nutritional Engineering, China Agricultural University, Beijing, China

ARTICLE INFO

Keywords:
Ochratoxin A
Bacillus subtilis
Tight junction
Toxicity
Apoptosis
Cell cycle

ABSTRACT

The multiple toxic effects of ochratoxin A (OTA) are a threat for human and animal. This study aimed to examine whether *B. subtilis* CW14 protected against OTA-induced barrier disruption and cell damage to Caco-2 cells. The results showed that Caco-2 cells treated with OTA led to microvilli disruption, tight junction protein (ZO-1 and claudin-1) damage, and inhibition of cell proliferation by arresting the cell cycle in the G2/M phase that promoted apoptosis. The treatment of *B. subtilis* CW14 mitigated the tight junction injury by improving ZO-1 protein expression, and it reduced apoptosis that was induced by OTA. Furthermore, transcriptome analysis indicated that OTA down-regulated genes that involved in the tight junction, cell cycle, and apoptosis-related signaling pathways. *B. subtilis* CW14 may have protected the ZO-1 protein by activating the toll-like receptor signaling pathway, and it reduced OTA damage by down-regulating the death receptor genes and up-regulating the DNA repair genes. These findings demonstrated the importance of *B. subtilis* CW14 in the regulation of tight junction proteins and in reducing death of intestinal epithelial cells. Thus, *B. subtilis* CW14 is a potential candidate as a food additive to protect against intestinal damage.

1. Introduction

Mycotoxin ochratoxin A (OTA) is a secondary metabolite secreted by various species of *Aspergillus* and *Penicillium*, which easily infects diverse agricultural products, such as cereals, coffee, and fruits (Wang et al., 2016). OTA is nephrotoxic, genotoxic, teratogenic, and immunotoxic (Malir et al., 2016). A number of mechanisms are involved in OTA toxicity, for instance, inhibition of protein synthesis, mitochondrial dysfunctions, inhibition of histone acetyltransferase, and formation of DNA adducts (Akbari et al., 2017). *In vitro*, toxic effects of OTA included impairing barrier function, inhibiting cellular proliferation, inducing DNA damage and apoptosis (Zhu et al., 2017). More recently, the adverse effects of OTA on the impairment of intestinal barrier function have been documented (Gao et al., 2018; Romero et al., 2016). Probiotics may improve epithelial barrier disruption and reduce cell damage that was induced by mycotoxins, such as aflatoxin and deoxynivalenol (Gratz et al., 2007; Gu et al., 2014). However, the exact effects and mechanisms of probiotics on OTA-induced epithelial barrier disruption and cell damage are not well understood.

Probiotics have been defined as living organisms that are present in food and dietary supplements, which have many beneficial effects, such as maintaining the normal intestinal milieu, modulating the immune system, and producing metabolites required for intestinal health (Eun et al., 2011; Teitelbaum and Walker, 2002). Specific strains of probiotics have some potential to maintain intestinal barrier function and to reduce cell damage after being impaired by cytokines, chemicals, or pathogens (Ahrne and Hagslatt, 2011). Probiotic *Lactobacillus* spp strengthened intestinal barrier function and tight junction integrity in intestinal epithelial cells (Caco-2 cells) (Blackwood et al., 2017). *L. casei* prevented cytokine-induced dysfunction of epithelial barrier in Caco-2 cells (Eun et al., 2011). *Bacillus subtilis* protected porcine intestinal barrier from deoxynivalenol by improving the expression of zonula occludens-1 (ZO-1) (Gu et al., 2014), and a quorum-sensing molecule of *B. subtilis* contributed to intestinal homeostasis by a host cell membrane transporter OCTN2 (Fujiya et al., 2007). In addition, *L. rhamnosus* GG modulated the intestinal mucosal barrier and inflammation in Balb/c mice that followed combined dietary exposure to deoxynivalenol and zearalenone (Wan et al., 2016b). Among all possible routes of modulation by probiotics of intestinal epithelial cell-mediated defense responses, regulation of intestinal barrier function and signaling

* Corresponding author. No.17 Qinghua East Road, Haidian District, Beijing, 100083, China.
E-mail address: lzh105@cau.edu.cn (Z. Liang).

https://doi.org/10.1016/j.fct.2019.02.009
Received 7 June 2018; Received in revised form 21 January 2019; Accepted 4 February 2019
Available online 11 February 2019
0278-6915/

pathways play an important role in the intestine's defense against mycotoxins (Wan et al., 2016a). Nevertheless, the effect of *B. subtilis* together with the signaling pathways on intestinal barrier function needs further investigation.

Inhibition of proliferation, cell cycle arrest, and apoptosis were important bioeffects of many carcinogenic mycotoxins (Du et al., 2017; Liu et al., 2015). Several studies have demonstrated that OTA induced DNA damage that led to cell death (Cui et al., 2010; Liu et al., 2015). Some mycotoxins, such as OTA, aflatoxins, fumonisin, and deoxynivalenol, affected cell cycle phases in human hepatoma cells (HepG2) (Du et al., 2017), porcine intestinal epithelial cells (IPEC-1) (Bouhet et al., 2004), and human esophageal epithelium cells (Het-1A) (Liu et al., 2015). In previous studies, probiotic lactic acid bacteria and *B. megaterium* affected the cell cycle phases and protected against mycotoxin-induced toxicity (Di Luccia et al., 2016; Khalil et al., 2015). However, whether *B. subtilis* CW14 can reduce OTA-induced DNA damage, apoptosis, and cell cycle arrest in Caco-2 cells remains unclear.

In our study, we hypothesized that the probiotic *B. subtilis* CW14 influenced the expression of tight junction proteins in Caco-2 cells that contributed to a protective effect against OTA-induced damage. Therefore, the aim of this study was to examine whether the *B. subtilis* CW14 strain protected against OTA-induced barrier disruption and cell damage in a human intestinal epithelial cell line (Caco-2). We also examined whether this strain protects its signaling pathways, as assessed by transcriptome analysis.

2. Materials and methods

2.1. Chemicals and reagents

OTA (purity > 98%) was purchased from Fermentek (Jerusalem, Israel). OTA was dissolved in dimethyl sulfoxide (DMSO) to a final concentration of 5 mg/mL and stored at −20 °C. Dulbecco's modified Eagle medium (DMEM), fetal bovine serum (FBS), antibiotics (100 units/mL penicillin and 100 μg/mL streptomycin), HEPES buffer, HBSS buffer, and nonessential amino acids (NEAA) were purchased from Corning (New York, USA). Rabbit anti-ZO-1 and rabbit anti-claudin-1 were purchased from Cell Signaling Technology (Trask Lane Danvers, USA). Goat anti-rabbit IgG conjugated to fluorescein isothiocyanate (FITC) was purchased from Solarbio (Beijing, China). Primary antibody dilution buffer and secondary antibody dilution buffer were purchased from Beyotime Biotechnology (Shanghai, China). An enhanced cell counting kit (CCK)-8, an annexin V-FITC cell apoptosis assay kit, and a cell cycle assay kit were purchased from Solarbio (Beijing, China). Transwell inserts with 0.4 μm pores and translucent polycarbonate membranes were purchased from Corning (New York, USA).

2.2. Bacterial strain and cell culture

Bacillus subtilis CW14 was obtained from our laboratory from previous work (Shi et al., 2014) and stored at −80 °C. The complete genome was deposited in GenBank under the accession number CP016767. *B. subtilis* CW 14 was incubated in LB-nutrient broth (10 g/L pancreatic peptone, 5 g/L yeast extract, and 10 g/L NaCl, pH 7.0) at 37 °C for 24 h. Then the concentration of *B. subtilis* CW14 was checked by colony forming units (CFU) that was counted on LB agar. The *B. subtilis* CW14 was centrifuged at 6000 × *g* for 5 min at 4 °C. After being washed twice with HBSS buffer, *B. subtilis* CW14 was suspended in HBSS, which resulted in a concentration of 1×10^{10} CFU/mL for OTA transport assays. *B. subtilis* CW14 was diluted to 10^2, 10^3,10^4, 10^5, 10^6, 10^7, 10^8, 10^9, and 10^{10} CFU/mL using cell culture medium without antibiotics for cell viability assays. The concentration of 10^4 CFU/mL of *B. subtilis* CW14 was used for immunofluorescent staining of tight junction proteins, cell cycle analysis, and apoptosis analysis.

The Caco-2 cell line was obtained from American Type Culture Collection (ATCC, HTB 37), which was isolated originally from a human colon adenocarcinoma. The cells were cultured in DMEM medium that contained 4.5 g/L glucose, 10% FBS, antibiotics (100 units/mL penicillin and 100 μg/mL streptomycin), 10 mM HEPES buffer, and 1% NEAA at 37 °C in a humidified atmosphere of 5% CO_2 in air. Control cells were incubated with DMSO (final solvent concentration 0.12%).

2.3. Transport assays

Caco-2 cells are routinely cultivated as monolayers on permeable filters. During culturing, they undergo spontaneous differentiation that results in polarization and formation of the tight junction proteins between adjacent cells (Akbari et al., 2017). Differentiated Caco-2 cells form polarized apical/mucosal and basolateral/serosal membranes that are impermeable, and they are structurally and functionally similar to epithelial cells of the small intestine (Akbari et al., 2017). Caco-2 cells were cultured and differentiated in 12-well transwell inserts at a density of 2×10^5 cells/cm^2, and the medium was replaced every other day within 7 d of cell inoculation, and then changed daily until 21 d. The alkaline phosphatase of spent medium was detected using the Alkaline Phosphatase Assay Kit (Beyotime, China) according to the manufacturer's instruction. The transepithelial electrical resistance (TEER) value was measured by a Millicell-ERS volt-ohm meter (Millipore, Temecula, USA). Only cell monolayers with a TEER value above 300 Ω cm^2 were used for transport assays of OTA.

OTA transport assays were carried out according to the protocol described by Hubatsch et al. (2007). HBSS that contained 10 mM HEPES was used as the transport buffer. Cell monolayers were pre-incubated with transport buffer and maintained at 37 °C until required. The volume of buffer in the apical (AP) and basolateral (BL) chambers was 0.5 mL and 1.5 mL, respectively. Transport assays were performed by adding 15 μmol/L OTA and/or 10^{10} CFU/mL *B. subtilis* CW14 to the AP chamber (0.5 mL/well). Transport buffers were collected from both compartments after 5 h. The OTA of transport buffers was analyzed by high performance liquid chromatography (HPLC). The transport ratio of OTA was calculated according to the following equation: Transport ratio (%) = 100% × (OTA content in BL/Total OTA content).

2.4. OTA extraction and detection

The OTA of transport buffers was extracted and detected using methods developed by Shi et al. (2014). Briefly, all samples were acidified with 2 mol/L HCl and extracted twice with 2 mL of chloroform. OTA was recovered by centrifugation of the extracts at 12000 × *g* for 5 min at 4 °C. The chloroform extracts were evaporated, re-dissolved with methanol, filtered using 0.22 μm cellulose pyrogen-free filters, and used for HPLC analysis. Then the OTA was detected by Institute of Agro-Products Processing Science and Technology, Chinese Academy of Agricultural Sciences (Beijing, China). The analysis was performed on BST Rutin C18 BD HPLC columns (250 mm × 4 mm, particle size 10 μm; Bio-Separation Techniques, Budapest, Hungary) that were coupled with a fluorescence detector (FD) at excitation and emission wavelengths of 334 and 460 nm, respectively. OTA was eluted at a flow rate of 1 mL/min of mobile phase (acetonitrile/water/acetic acid 99:99:1). Quantification of OTA was performed by measuring the peak area and comparing it to the respective OTA calibration curve ($y = 165355\ x - 787826$, $R^2 = 0.9998$).

2.5. Transmission electron microscope

The microvilli and tight junction structure of Caco-2 monolayers were observed by a transmission electron microscope (TEM) (Yang et al., 2008). The Caco-2 monolayers were incubated with 15 μM OTA and/or 10^{10} CFU/mL *B. subtilis* CW14 for 5 h. Then the Caco-2 monolayers were washed three times with 0.1 mol/L sterile PBS (pH 7.4) and fixed in cold (4 °C) 2.5% glutaraldehyde and 0.1 mol/L PBS overnight.

These cell monolayers were post-fixed in cold 1% OsO_4 in 0.1 mol/L phosphate buffer for 60 min and then rinsed twice with 0.1 mol/L PBS. After dehydrating through a graded series of alcohol, the cells were embedded in epoxy resin SPURR. The cells were sectioned and stained with uranyl acetate and lead citrate and observed with a JEM-1230 electron microscope (JEOL, Tokyo, Japan).

2.6. Immunofluorescent staining

The localization of tight junction proteins (ZO-1 and claudin-1) was assessed by a fluorescence microscope. The cells were seeded at a density of 5×10^5 cells/well in a 6-well plate for 24 h. Confluent Caco-2 cells were incubated for 24 h with 30 μM OTA and/or 10^4 CFU/mL *B. subtilis* CW14. The cells were washed twice with PBS and fixed with 4% paraformaldehyde for 10 min and then permeabilized with 0.1% Triton X-100 in PBS for 5 min. The cells were incubated in 5% bovine serum albumin (BSA) for 1.5 h at 37 °C followed by incubation with rabbit anti-ZO-1 or rabbit anti-claudin-1 that was diluted in primary antibody dilution buffer for 24 h at 4 °C in the dark. The cells were then incubated with goat anti-rabbit IgG that was diluted in secondary antibody dilution buffer for 2 h at 37 °C in the dark. The cells were observed under a fluorescence microscope (Axio Vert A1, Carl Zeiss, German).

2.7. Cell viability assays

The effect of OTA on the proliferation of Caco-2 cells was determined using a CCK-8 (Tominaga et al., 1999), according to the manufacturer's instructions. The cells were seeded at 6×10^4 cells/well in 100 μL of complete proliferation medium in 96-well plates. After 24 h of culture the cells reached 70%–80% confluency. Culture medium without antibiotic that contained OTA (0.1–30 μM) and/or *B. subtilis* CW14 (10^2–10^{10} CFU/mL) was used to treat the cells for 24 h. Then we abandoned the spent medium, added new DMEM medium that contained antibiotics, and continued culturing for 1 h. Then, 10 μL of CCK-8 reagent was added per well, and the cells were incubated for 2 h. The optical density (OD) was measured at 450 nm using an automated ELISA reader (Thermo Scientific, Waltham, USA). Results were expressed as cell survival (%) with respect to the control [(OD_{450} treated wells/OD_{450} control wells) × 100%].

Based on the cell viability assays, and after incubation with Caco-2 cells for 24 h, 30 μM of OTA caused the greatest damage to Caco-2 cells, and the *B. subtilis* CW14 with $< 10^5$ CFU/mL caused no significant toxicity to Caco-2 cells. To determine whether *B. subtilis* CW14 reduced OTA-induced damage, Caco-2 cells that were exposed previously to 30 μM of OTA and/or 10^4 CFU/mL of *B. subtilis* CW14 for 24 h were subjected to immunofluorescent staining of tight junction proteins, cell cycle analysis, and apoptosis analysis.

2.8. Flow cytometry analysis

The cell cycle and apoptosis of Caco-2 cells were analyzed by flow cytometry. The cells were seeded at a density of 5×10^5 cells/well in a 6-well plate for 24 h. Confluent Caco-2 cells were incubated for 24 h with 30 μM OTA and/or 10^4 CFU/mL *B. subtilis* CW14. Then, the cell cycle was analyzed using the propidium iodide (PI) dye that can bind double strand DNA (Pozarowski and Darzynkiewicz, 2004). The PI staining solution contained RNase A. Cell apoptosis was analyzed by employing a staining reagent of PI and Annexin V-FITC, as described by Vermes et al. (1995). Flow cytometry (FACSCalibur, BD Biosciences, Franklin Lakes, USA) with Multi-Cycle AV software was used to analyze the cell cycle and apoptosis rates.

2.9. Transcriptome analysis

After the transport studies of OTA, Caco-2 cells were collected for transcriptome analysis. The mRNA sequences were determined by Geek Gene Technology (Beijing, China) using an Illumina (HISeq X Ten) Platform. Total RNA was extracted using a RNeasy Micro Kit (QIAGEN, 74004). Extracted RNA was quantified with a Qubit RNA Assay Kit (Invitrogen). Further mRNA library construction was performed with a NEB Next Ultra RNA Library Prep Kit for Illumina (NEB, E7530) by following instructions in the manuals. The libraries were sequenced on Illumina Hiseq X Ten instruments with 150bp pair-end reads. All clusters that passed the quality filter were exported into fastq files. Raw RNA-seq reads were trimmed using adaptor sequences, and low-quality reads were removed using Cutadapt (v1.10). Reads were then aligned to the hg19 reference genome using Tophat2 (v2.0.13). Reads aligned to genes were counted by Cufflinks (v2.2.1), and the FPKMs were normalized using Cuffnorm. Differentially expressed genes (DEGs) were calculated using Cuffdiff. Then, the identified DEGs were performed Kyoto Encyclopedia of Genes and Genomes (KEGG) pathway enrichment analyses using Database for Annotation, Visualization, and Integrated Discovery (DAVID), which is an online tool (http://david.abcc.ncifcrf.gov/). When different treatment samples were compared, genes were considered differentially expressed if their expression differed by more than a 2-fold change with a significance of q-value < 0.05. The high-throughput functional genomics data used in this study were deposited in the NCBI Gene Expression Omnibus database (GEO: http://www.ncbi.nlm.nih.gov/geo/) under the accession number GSE115081.

2.10. Statistical analysis

Data were expressed as mean ± standard deviation of three independent experiments. All data analyses were performed using the SPSS statistical package (SPSS Version 20.0, USA). One-way ANOVA with Duncan's multiple comparison test were used for the analysis of parametric data. Data with different lowercase letters were considered to be significantly different ($p < 0.05$).

3. Results

3.1. Establishment of the Caco-2 cell monolayer model

Caco-2 cells are routinely cultivated as monolayers on permeable filters. During culturing, they undergo spontaneous differentiation that results in polarization and formation of the tight junction proteins between adjacent cells. Differentiated Caco-2 cells form polarized apical/mucosal and basolateral/serosal membranes that are impermeable and are structurally and functionally similar to epithelial cells of the small intestine.

The transmission electron micrographs of characteristic microvilli and tight junction structure on the apical side of the differentiated Caco-2 monolayers after 21 d of culture showed that the brush edges formed by the microvilli arranged neatly and densely (Fig. 1A). The AP side differentiated into a complete tight junction structure, which indicated that the Caco-2 monolayers were similar morphologically to intestinal epithelial cells.

The TEER across epithelial cell monolayers is one of the key parameters to estimate the integrity of the tight junction barrier in Caco-2 monolayer models and to qualify the model for use in the transportation experiment (Fig. 1B). After seeding, TEER values of the monolayers that developed in this study increased steadily over time and were > 500 $\Omega\,cm^2$ on day 21, which demonstrated that the Caco-2 cell monolayer had formed a complete and dense tight junction structure.

AKPase is one of the brush border enzyme markers that indicates the polarization of the cell membrane of Caco-2 monolayers. With an increase in culture time, the AKPase activity on the AP side increased gradually, but the BL side changed only slightly (Fig. 1C). After 21 d of culture, the activity of AKPase on the AP side was five times greater than on the BL side. This demonstrated that the differentiated Caco-2 cells had obvious polarity, and the appearance of brush borders was

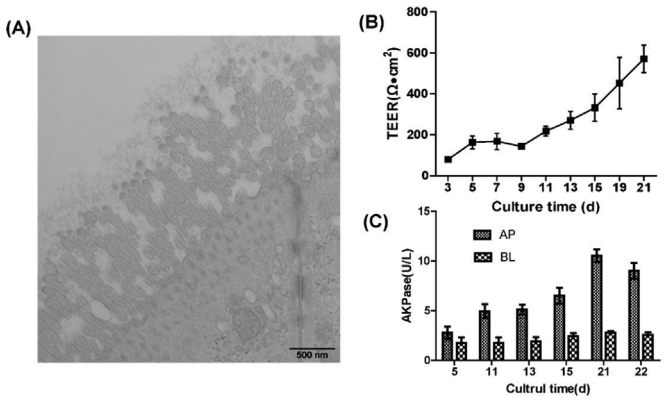

Fig. 1. Establishment of Caco-2 cell monolayer model. (A) Characteristic microvilli and tight junction structure of apical side of the differentiated Caco-2 monolayer. (B) TEER values of the developing Caco-2 cell monolayers. (C) AKPase activity of the developing Caco-2 cell monolayers at apical (AP) and basolateral (BL) chambers.

accompanied by the production of alkaline phosphatase. In summary, Caco-2 cells cultured in the transwell inserts for 21 d exhibited similar structures and functions as those of small intestine epithelial cells, which indicated that the Caco-2 cell monolayer model was established successfully.

3.2. Microvilli was damaged during OTA transport

Based on the cell viability assays, Caco-2 cells that were treated with 15 μM of OTA and/or 10^{10} CFU/mL of *B. subtilis* CW14 for 5 h caused no significant cytotoxicity (Data are shown in Supplementary Fig. S1). To determine the effect of OTA and *B. subtilis* CW14 on the monolayer structure of Caco-2 cells and the effect of *B. subtilis* CW14 on OTA transport, OTA (15 μM) and *B. subtilis* CW14 (10^{10} CFU/mL) were added separately or together to the Caco-2 cell monolayers. We then observed the cell monolayer structure by transmission electron microscopy and measured the OTA content of the transport buffer at the apical and basolateral chambers using HPLC-FD (Fig. 2).

In the control group, microvilli on the cell surface were distributed evenly and arranged neatly, with the same length and direction; the tight junction structure between cells was intact and densely connected (Fig. 2A). However, in the OTA treatment group, the microvilli on the cell surface were reduced significantly, varied in length, were distributed unevenly, and disordered (Fig. 2B). Surprisingly, there was little microvilli damage in the *B. subtilis* CW14 treatment group (Fig. 2C). In the OTA and *B. subtilis* CW14 co-treatment groups, microvilli structure was damaged seriously (Fig. 2D). No significant changes were observed in the tight junction structure among all treatment groups.

The transport ratio of OTA from AP to BL was investigated over a period of 5 h, and it was calculated from the concentrations of OTA in the AP and BL compartments (Fig. 2E and F). The transport ratios of OTA alone or in combination with *B. subtilis* CW14 were 25.38% and 32.92% respectively, although there was no significant difference, which suggested that *B. subtilis* CW14 did not prevent the transport of OTA. There was no significant difference in OTA concentration on the AP side with OTA alone or in combination with *B. subtilis* CW14, which suggested that the permeability of Caco-2 cells was the same (Fig. 2E). Compared with OTA alone, OTA combined with *B. subtilis* CW14 had a high OTA concentration on the BL side, which suggested that *B. subtilis* CW14 promoted the transport of OTA by the BL side transporters of Caco-2 cells.

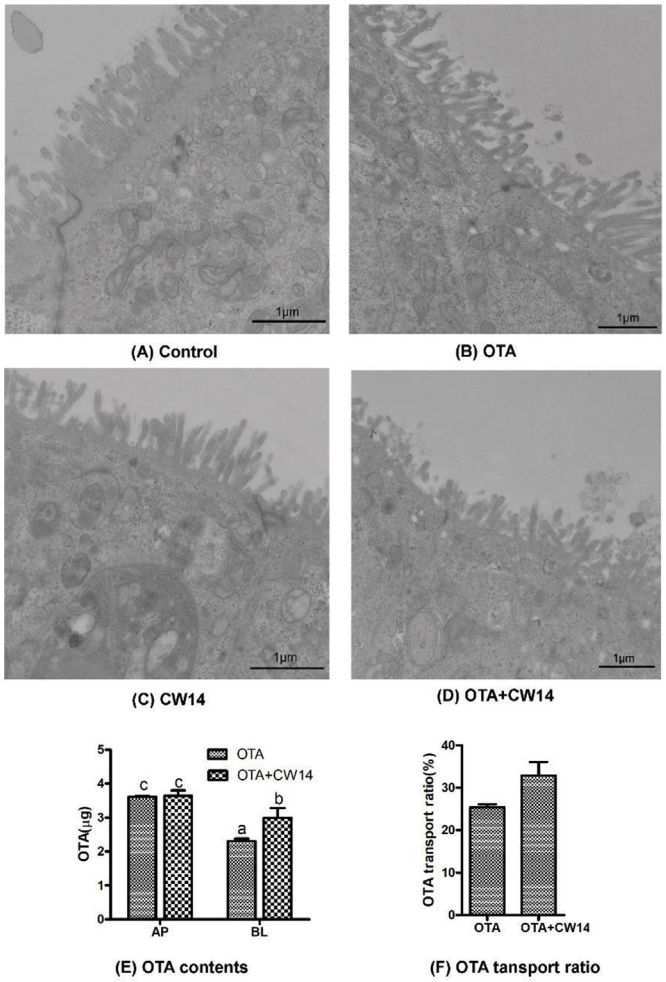

Fig. 2. The characteristic structure on the apical side of the differentiated Caco-2 monolayers and the transport ratio of OTA. The Caco-2 monolayers were treated with 15 μM OTA and 10^{10} CFU/mL *B. subtilis* CW14 alone or in combination for 5 h. (A) The cells were treated with DMSO. (B) The cells were treated with OTA. (C) The cells were treated with *B. subtilis* CW14. (D) The cells were treated with OTA and *B. subtilis* CW14 combined. (E) The contents of OTA at the apical and basolateral chambers. (F) OTA transport ratio. The micrographs were observed by TEM. Values are means with the standard deviation of three independent experiments (n = 3). Data with different lowercase letters were considered to be significantly different ($p < 0.05$) by Duncan's multiple comparison test.

3.3. B. subtilis CW14 reduced the tight junction damage that was induced by OTA

To investigate the effect of OTA and *B. subtilis* CW14 on the tight junction of Caco-2 cells, the localization and distribution of tight junction proteins (ZO-1 and claudin-1) were observed by a fluorescence microscope (Fig. 3). ZO-1 protein distributed mainly along the cell membrane. In the control group and *B. subtilis* CW14 treatment group, ZO-1 showed a honeycomb shape that arranged closely with smooth edges, which resembled typical paving stones in Caco-2 cells (Fig. 3A). However, after treatment with 30 μM of OTA for 24 h, the ZO-1 network pattern had an uneven distribution in the fluorescence signal, a weakened fluorescence intensity, and breakage of junctions (Fig. 3A). Compared with the OTA treatment group, the OTA and *B. subtilis* CW14 co-treatment partially repaired the reduction of the ZO-1 fluorescence intensity caused by OTA treatment alone, and more intense fluorescence appeared at the intersection of multiple cells, which indicated that the cell gap had increased (Fig. 3A).

The claudin-1 fluorescence signal of the control group was

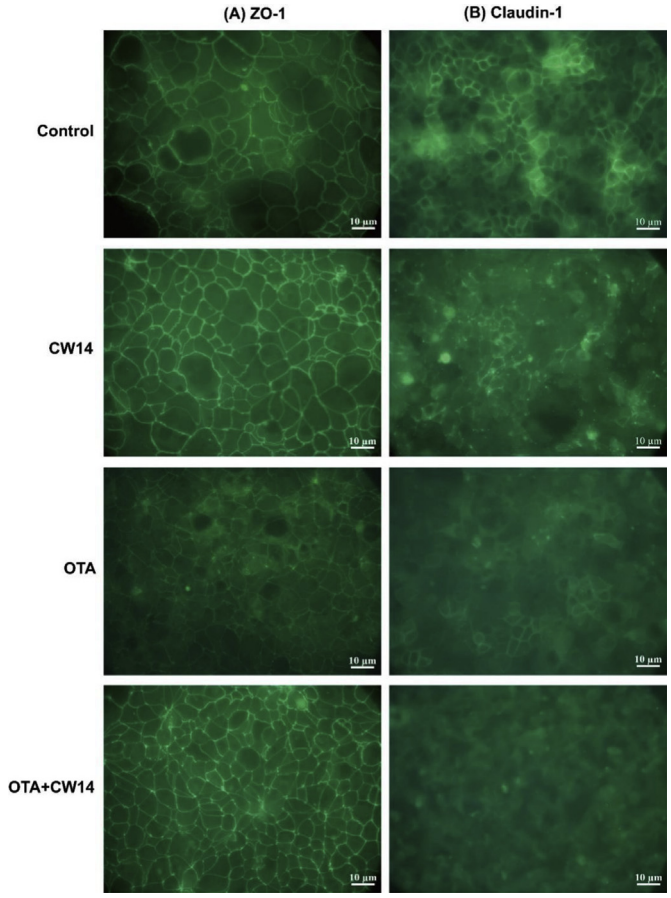

Fig. 3. Localization and distribution of tight junction proteins. The cells were treated with 30 μM OTA and/or 10^4 CFU/mL *B. subtilis* CW14 for 24 h. (A) ZO-1 of Caco-2 cells. (B) Claudin-1 of Caco-2 cells. The micrographs were taken under fluorescence microscopy.

distributed in the cytoplasm of the proximal cell membrane, which formed a dense ring structure with smooth and continuous edges (Fig. 3B). Both OTA and *B. subtilis* CW14 reduced the fluorescence intensity of claudin-1, and the negative effect of *B. subtilis* CW14 and OTA in combination was greater than those of *B. subtilis* CW14 and OTA individually (Fig. 3B). Taken together, the immunofluorescence observations of ZO-1 and claudin-1 indicated that OTA had a destructive effect on tight junction proteins, and *B. subtilis* CW14 partially protected the OTA-induced damage to ZO-1. The effect of *B. subtilis* CW14 on the tight junction proteins was two-sided. It not only protected ZO-1, but it also destroyed claudin-1, which reflected the complexity of the interaction mechanism between *B. subtilis* CW14 and tight junction proteins.

3.4. *B. subtilis CW14 mitigated the toxicity of OTA to Caco-2 cells*

Cell viability is one of the most important parameters that reflects the state of cell growth. The effect of OTA and/or *B. subtilis* CW14 treatment on cell viability was assessed by employing CCK-8 assays. Exposure to OTA (0.1–30 μM) induced a concentration-dependent decrease in cell viability, and OTA alone or in combination with 10^4 CFU/mL of *B. subtilis* CW14 showed no significant difference (Fig. 4A). At the highest concentration level of OTA studied (30 μM, 24 h), cell viability was 68.1 ± 2.4%. The inoculation concentration of *B. subtilis* CW14 of $< 10^5$ CFU/mL exhibited no significant cytotoxicity to Caco-2 cells, but at a seeding concentration of $> 10^5$ CFU/mL, the cytotoxicity increased dramatically (Fig. 4 A).

The effect of OTA in the Caco-2 cell cycle was investigated by assessing the cell's DNA content using PI stain in fixed cells (Fig. 4B). The cell cycle distribution of the *B. subtilis* CW14 treated group (10^4 CFU/mL, 24 h) was similar to that of the control cells. However, the exposure to OTA (30 μM, 24 h) resulted in an increase in the G2/M population (14.6%). The combined exposure to OTA and *B. subtilis* CW14 led to a significant reduction in the G0/G1 population (30.5%) and a remarkable increase in the S population (41.7%) compared with OTA exposure (Fig. 4B).

The occurrence of apoptosis was confirmed further by double staining of live cells with Annexin V-FITC and PI (Fig. 4C). *B. subtilis* CW14 (10^4 CFU/mL, 24 h) exposure alone did not change the apoptosis population compared with non-treated control cells. However, apoptosis of Caco-2 cells exposed to OTA (30 μM, 24 h) increased 25.6% (Fig. 4C). The combined exposure of *B. subtilis* CW14 and OTA led to a minor decrease in the apoptosis population compared with the cells exposed only to OTA.

3.5. *OTA down-regulated gene expression that was involved in tight junctions, cell cycle, and apoptosis-related pathways*

To determine the mechanisms that underlie OTA-induced barrier disruption and cell damage and the protective mechanisms of *B. subtilis* CW14 on cells, Caco-2 cells were collected after the transport assays for transcriptome analysis. The Caco-2 cells were treated with *B. subtilis* CW14 (10^{10} CFU/mL), OTA (15 μM), and OTA (15 μM) in combination with 10^{10} CFU/mL of *B. subtilis* CW14 for 5 h, and compared with the control group, there were 23, 1014, and 937 up-regulated genes and 67, 143, and 629 down-regulated genes, respectively (using the filtering criteria: fold change > 2, and q-value < 0.05). We performed KEGG pathway enrichment analyses to map the DEGs to the KEGG metabolic and regulatory pathways. The main enriched pathways were: apoptosis, cell cycle, gap junction, endocytosis, regulation of actin cytoskeleton, ErbB signaling pathway, foxO signaling pathway, hippo signaling pathway, jak-STAT signaling pathway, MAPK signaling pathway, NF-kappa B signaling pathway, NOD-like receptor signaling pathway, p53 signaling pathway, PI3K-Akt signaling pathway, rap1 signaling pathway, ras signaling pathway, RIG-I-like receptor signaling pathway, TGF-beta signaling pathway, TNF signaling pathway, and Toll-like receptor (TLR) signaling pathway (Fig. 5A). These pathways are mainly related to cell proliferation, differentiation, survival, and transport of substances. The OTA treatment and the co-treatment of OTA and *B. subtilis* CW14 activated more signaling pathways than the *B. subtilis* CW14 treatment alone, which reflected the toxicity of OTA to Caco-2 cells.

In the tight junction and cell cycle pathways (Fig. 5B and D), there was no significant difference in gene expression between the control group and the *B. subtilis* CW14 treatment group. In addition, compared with the OTA treatment and the OTA and *B. subtilis* CW14 co-treatment groups, the DEGs of the *B. subtilis* CW14-treated group were also less common in the apoptotic pathway (Fig. 5E), which indicated that *B. subtilis* CW14 was less damaging to Caco-2 cells. However, OTA treatment down-regulated the expression of most genes that were involved in cell apoptosis, cell cycle, tight junction, and the TLR signaling pathways, which suggested that Caco-2 cells were damaged by OTA.

Based on the analysis of DEGs, OTA disrupted the tight junction structure of Caco-2 cells by down-regulating the expression of tight junctional pathway genes (Fig. 5B), such as ZO-1 (TJP1), claudin-23 (CLDN23) and claudin-4 (CLDN4), and occludin (OCLN). The TLR signaling pathway is involved in epithelial cell proliferation and maintenance of tight junctions (Kuo et al., 2013), which is crucial for maintaining a healthy epithelial barrier. We found that OTA treatment down-regulated the TLR signaling pathway genes (Fig. 5C), such as cathepsin K (CTSK), C-X-C motif chemokine ligand (CXCL10), interleukin 12A (IL12A), mitogen-activated protein kinase kinase kinase 8 (MAP3K8), NFKB inhibitor alpha (NFKBIA), phosphoinositide-3-kinase regulatory subunit 3 (PIK3R3), receptor interacting serine/threonine kinase 1 (RIPK1), TANK binding kinase 1 (TBK1), toll-like receptor

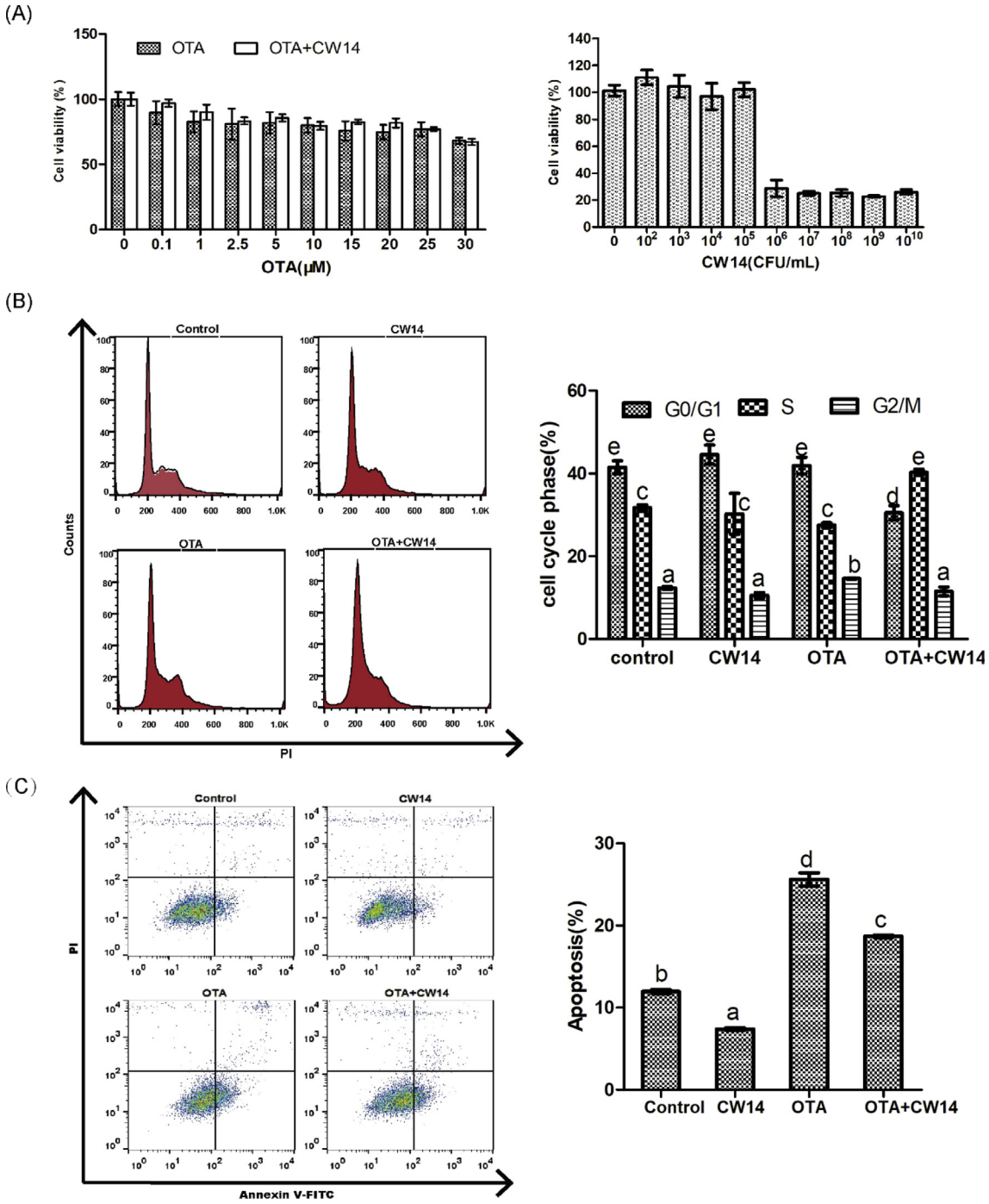

Fig. 4. Effect of OTA and *B. subtilis* CW14 on cell viability, cell cycle progression, and apoptosis of Caco-2 cells. (A) The viability of Caco-2 cells. The cells were treated with OTA (0.1–30 μM), *B. subtilis* CW14 (10^2–10^{10} CFU/mL), and OTA (0.1–30 μM) in combination with 10^4 CFU/mL of *B. subtilis* CW14 for 24 h. (B) The cell cycle progression. The cells were treated with 30 μM OTA and/or 10^4 CFU/mL *B. subtilis* CW14 for 24 h. According to the flow cytometry histograms, the graph summarized the cell populations at different phases. (C) The apoptosis of Caco-2 cells. The cells were treated with 30 μM OTA and/or 10^4 CFU/mL *B. subtilis* CW14 for 24 h. The percentage of apoptotic cells (included early and late apoptotic cells) were summarized based on the flow cytometry dot-plots. Values are means with the standard deviation of three independent experiments (n = 3). Data with different lowercase letters were considered to be significantly different at $p < 0.05$ by Duncan's multiple range test.

adaptor molecule 1 (TICAM1), and TNF receptor associated factor 6 (TRAF6). *B. subtilis* CW14 treatment up-regulated the expression of TLR pathway genes, such as C-X-C motif chemokine ligand (CXCL8 and CXCL10), interleukin 1 beta (IL1B), NFKB inhibitor alpha (NFKBIA), toll like receptor adaptor molecule 1 (TICAM1), and tumor necrosis factor (TNF), which indicated that *B. subtilis* CW4 has the potential to protect the epithelial barrier through the TLR pathway.

In addition, OTA treatment caused cell cycle arrest by down-regulating the following genes (Fig. 5D): G2 checkpoint kinase (WEE1), growth arrest and DNA damage inducible alpha (GADD45A, GADD45B, and GADD45G), cyclin dependent kinase inhibitor (CDKN), cell division cycle (CDC), and cyclin E2 (CCNE2). The treatment of *B. subtilis* CW14 increased the gene expression of the minichromosome maintenance complex component (MCM2, MCM3, and MCM5) that maintain chromosomal stability, which suggested that *B. subtilis* CW14 has a protective effect on chromosomes. Furthermore, OTA down-regulated the

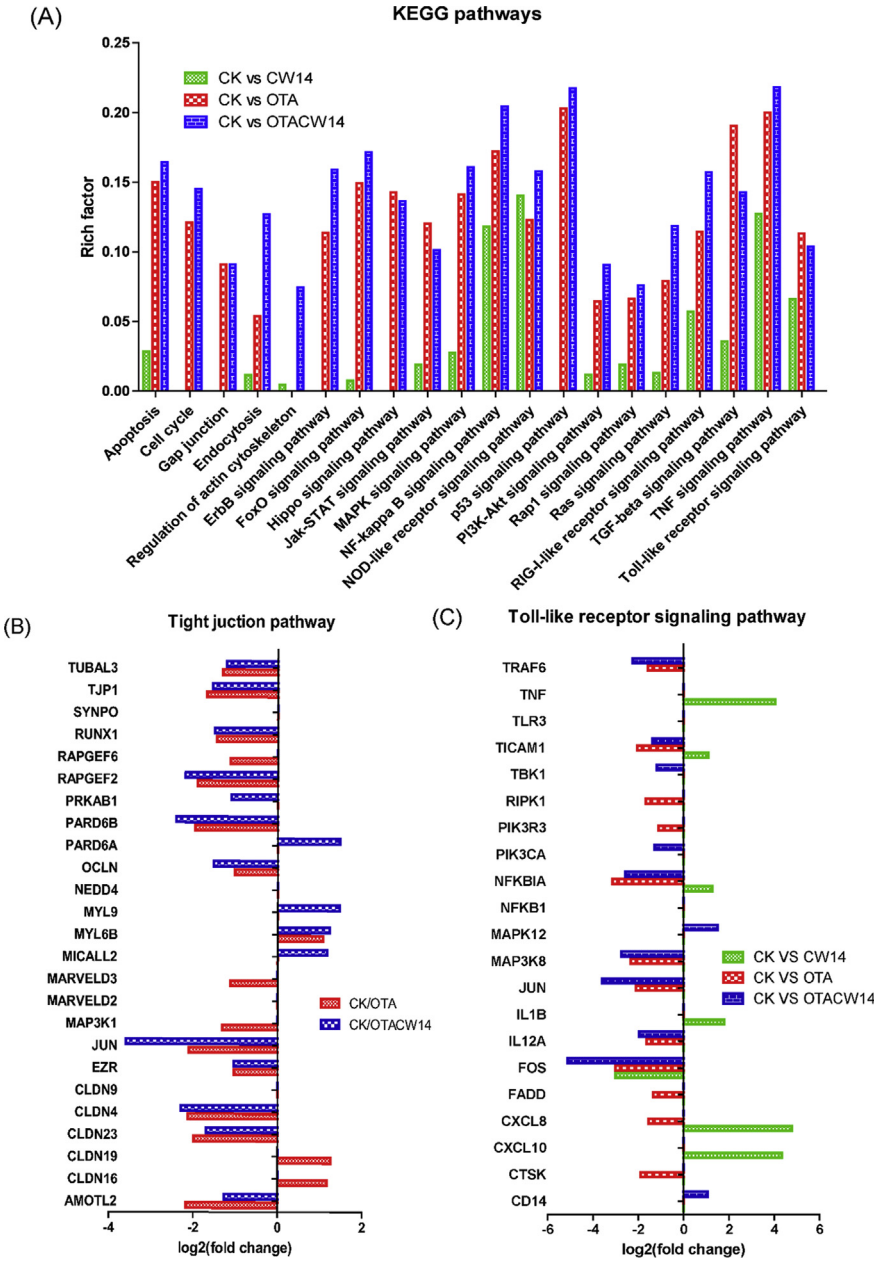

Fig. 5. The KEGG pathway enrichment of DEGs of Caco-2 cells. The cells were exposed to 15 μM OTA and/or 10^{10} CFU/mL *B. subtilis* CW14 for 5 h. (A) The enriched pathways of DEGs. (B) Expression of key genes related to tight junction pathway. (C) Expression of key genes related to Toll-like receptor pathway. (D) Expression of key genes related to cell cycle pathway. (E) Expression of key genes related to apoptosis pathway. Fold-changes are indicated for each gene that was significantly up- or down-regulated (fold-changes > 2, q-value < 0.05).

expression of apoptosis-related genes (Fig. 5E): fas associated with death domain (FADD), AP-1 transcription factor subunits (FOS and JUN), BCL2-associated regulators (BBC3, BCL2L1, BCL2L11, and MCL1), and DNA damage inducible transcript 3 (DDIT3). The accretion of *B. subtilis* CW14 up-regulated the DNA repair enzyme of poly (ADP-ribose) polymerase 1 (PARP1) and DNA fragmentation factor subunit alpha (DFFA). Taken together, OTA damaged Caco-2 cells by causing cell cycle arrest and triggering apoptosis; the coincubation of *B. subtilis* CW14 did not completely reduce those lesions, but it partially repaired OTA damage by maintaining chromosome and DNA stability.

4. Discussion

Probiotics prevented dysfunction of the intestinal epithelial barrier to maintain the integrity of the cell monolayer (Lodemann, 2010). In this study, we present evidence that OTA treatment of Caco-2 cells led to disruption of microvilli, damage to tight junction proteins (ZO-1 and claudin-1), and inhibition of cell proliferation by arresting the cell cycle in the G2/M phase that promoted apoptosis. Coincubation of *B. subtilis* CW14 strains mitigated injury to the tight junction, maintained genome stability, and reduced apoptosis that was induced by OTA.

The intestinal barrier has been an emerging target in the toxicological assessment of mycotoxins (Akbari et al., 2017). The Caco-2 cell line is well accepted as a reference model to conduct transport studies and to investigate the effects on barrier function (Akbari et al., 2017). Damage to microvilli and tight junctions alters the OTA transport pathways and transport ratio. The results of our transport assays indicated that OTA impaired the microvilli structure of the Caco-2 cell monolayers, and the co-treatment of *B. subtilis* CW14 did not reduce this damage (Fig. 2). The KEGG enriched pathways of DEGs revealed that

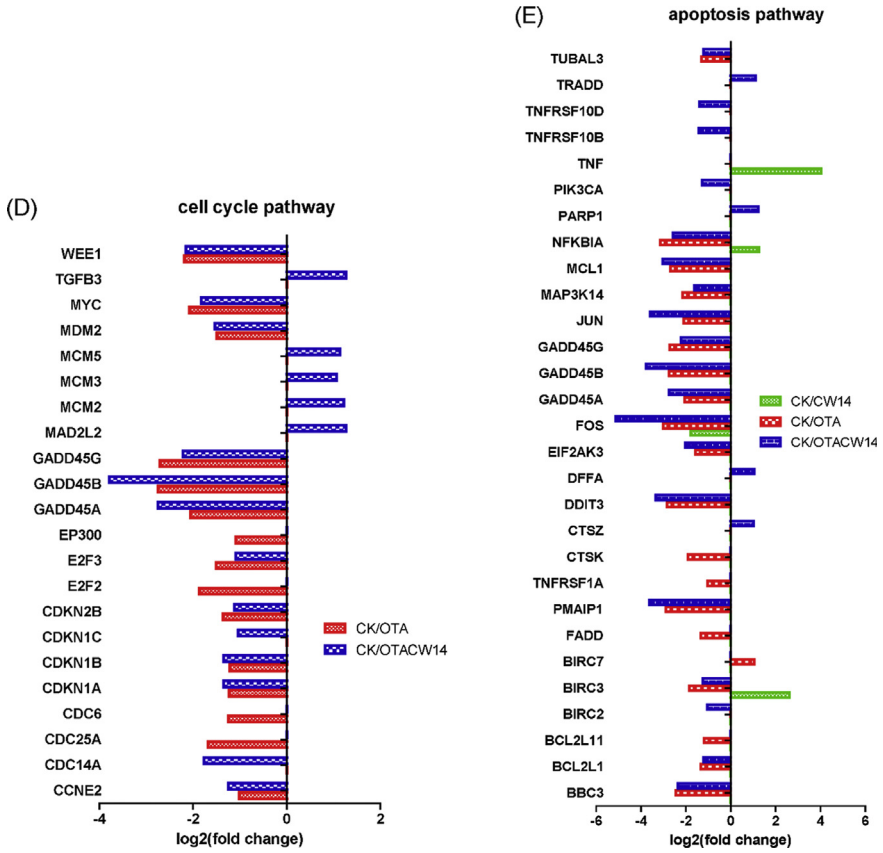

Fig. 5. (*continued*)

OTA exposure activated the gene expression in endocytosis and the intercellular signaling pathway (Fig. 5A), which suggested that Caco-2 cells transported OTA into the cell through endocytosis and by-passed transport through the intercellular space.

ZO-1 that interacted with claudins, occludins, and actin played an important role in the structural organization of tight junctions (Suzuki, 2013). OTA impaired the expression of tight junction proteins, and *B. subtilis* CW14 protected against a decline in ZO-1 expression (Fig. 3), which was similar to the findings of Gu et al. (2014) that *B. subtilis* protected the porcine intestinal barrier from deoxynivalenol by improving ZO-1 expression. Although our study also discovered that *B. subtilis* CW14 down-regulated the expression of claudin-1 (Fig. 3), claudin is not always necessary for the function of tight junctions (Cario et al., 2004). Toll-like receptor 2 ligands may enhance epithelial barrier function in humans and mice (Abreu, 2010; Kuo et al., 2013). Our transcriptome analysis revealed that OTA treatment down-regulated the TLR signaling pathway, but the *B. subtilis* CW14 treatment improved it, which indicated that *B. subtilis* CW4 has the potential to protect the epithelial barrier through the TLR pathway.

Cell cycle, which is the most important biological process, is divided into G0, G1, S, G2, and M phases. The G0/G1 phase restriction point and the G1/S and G2/M checkpoints ensure the stability of the genome. When the cell cycle is arrested, cellular apoptosis is likely to be the final fate of the reduction in cell proliferation (Du et al., 2017). We observed that exposure to OTA (0.1–30 μM, 24 h) induced a concentration-dependent decrease in cell viability, which was very similar to the research in other cell lines (Gao et al., 2018; Zhou et al., 2017). The exposure to OTA (30 μM, 24 h) led to an increase in the G2/M population (Fig. 4), which suggested that the G2/M checkpoint had found errors in DNA replication and, thus, blocked the progression of the cell cycle. The combined exposure to OTA and *B. subtilis* CW14 led to a significant reduction in the G0/G1 and G2/M populations and a remarkable increase in the S population when compared to OTA exposure alone. The main activities of S phase cells are DNA replication and DNA damage repair. According to the transcriptome analysis (Fig. 5), the DNA repair enzyme gene (PARP1) and the minichromosome maintenance complex component in the *B. subtilis* CW14 and OTA co-treated groups was up-regulated, which suggested that *B. subtilis* CW14 had a protective effect on chromosome stability. Depending on the cell types and OTA exposure conditions, different alterations in the cell cycle were observed in different studies, which included arrest in the G0/G1 (Kumar et al., 2012), S (Yang et al., 2014), and G2/M phases (Cui et al., 2010; Foellmann et al., 2014; Liu et al., 2015). This suggested that damaging DNA and causing cell cycle arrest may be one of the toxic mechanisms of OTA to Caco-2 cells.

OTA inhibited cell growth and induced cell death in various cell types (Gan et al., 2017; Ramyaa and Padma, 2013). In our study, Caco-2 cells exposed to OTA (30 μM; 24 h) showed increased apoptosis, and the co-treatment of *B. subtilis* CW14 decreased apoptosis that was induced by OTA (Fig. 4). Analysis of DEGs showed that OTA induced the down-regulation of genes that inhibited apoptosis and the tubulin genes that caused damage to microtubule function that eventually induced apoptosis (Fig. 5). The coincubation of *B. subtilis* CW14 down-regulated the TRAIL death receptor genes (TNFRSF10B and TNFRSF10D) and up-regulated the DNA repair genes (PARP1 and DFFA), which suggested that *B. subtilis* CW14 had an inhibitory effect on OTA-induced apoptosis. Many probiotics have been found to be effective against mycotoxin-induced toxicity and DNA-fragmentation, such as lactic acid bacteria (Khalil et al., 2015), *B. subtilis* (Ye et al., 2013), and *L. acidophilus* (Yanagihara et al., 2012). Taken together, *B. subtilis* CW14 protected the tight junction proteins, maintained DNA stability, and inhibited apoptosis so that it resisted OTA-induced cell damage.

5. Conclusion

In conclusion, our study demonstrated that OTA treatment of Caco-

2 cells led to disruption of microvilli, damage to tight junction proteins (ZO-1 and claudin-1), and inhibition of cell proliferation by arresting the cell cycle in the G2/M phase that promoted apoptosis. The co-treatment with the *B. subtilis* CW14 strain mitigated tight junction injury, maintained genome stability, and reduced apoptosis that was induced by OTA. These findings suggest an important role for *B. subtilis* in the regulation of tight junction proteins and reduction of cell death in intestinal epithelial cells. It is a potential candidate as a food additive to protect against intestinal damage. Further study of the mechanism used by *B. subtilis* CW14 to reduce OTA-induced injury is warranted.

Conflicts of interest

All authors declare that there is no conflict of interests.

Acknowledgments

The authors are grateful to the grant from the National Natural Science Foundation of China (Grant No.: 31671947). The authors would like to thank Prof. Jianfen Liang and Prof. Fazheng Ren from College of Food Science and Nutritional Engineering at China Agricultural University, for giving us the Caco-2 cell line and offering us the fluorescence microscope respectively.

Appendix A. Supplementary data

Supplementary data to this article can be found online at https://doi.org/10.1016/j.fct.2019.02.009.

Transparency document

Transparency document related to this article can be found online at https://doi.org/10.1016/j.fct.2019.02.009.

References

Abreu, M.T., 2010. Toll-like receptor signalling in the intestinal epithelium: how bacterial recognition shapes intestinal function. Nat. Rev. Immunol. 10 (2), 131–144.
Ahrne, S., Hagslatt, M.L., 2011. Effect of *Lactobacilli* on paracellular permeability in the gut. Nutrients 3 (1), 104–117.
Akbari, P., Braber, S., Varasteh, S., Alizadeh, A., Garssen, J., Fink-Gremmels, J., 2017. The intestinal barrier as an emerging target in the toxicological assessment of mycotoxins. Arch. Toxicol. 91 (3), 1007–1029.
Blackwood, B.P., Yuan, C.Y., Wood, D.R., Nicolas, J.D., Grothaus, J.S., Hunter, C.J., 2017. Probiotic *Lactobacillus* species strengthen intestinal barrier function and tight junction integrity in experimental necrotizing enterocolitis. J. Prob. Health 5 (1), 1–10.
Bouhet, S., Hourcade, E., Loiseau, N., Fikry, A., Martinez, S., Roselli, M., Galtier, P., Mengheri, E., Oswald, I.P., 2004. The mycotoxin fumonisin B-1 alters the proliferation and the barrier function of porcine intestinal epithelial cells. Toxicol. Sci. 77, 165–171.
Cario, E., Gerken, G., Podolsky, D.K., 2004. Toll-like receptor 2 enhances ZO-1-associated intestinal epithelial barrier integrity via protein kinase C. Gastroenterology 127, 224–238.
Cui, J., Xing, L., Li, Z., Wu, S., Wang, J., Liu, J., Wang, J., Yan, X., Zhang, X., 2010. Ochratoxin A induces G(2) phase arrest in human gastric epithelium GES-1 cells *in vitro*. Toxicol. Lett. 193, 152–158.
Di Luccia, B., D'Apuzzo, E., Varriale, F., Baccigalupi, L., Ricca, E., Pollice, A., 2016. *Bacillus megaterium* SF185 induces stress pathways and affects the cell cycle distribution of human intestinal epithelial cells. Benef. Microbes 7 (4), 609–620.
Du, M., Liu, Y., Zhang, G., 2017. Interaction of aflatoxin B-1 and fumonisin B-1 in HepG2 cell apoptosis. Food Bioscience 20, 131–140.
Eun, C.S., Kim, Y.S., Han, D.S., Choi, J.H., Lee, A.R., Park, Y.K., 2011. *Lactobacillus casei* prevents impaired barrier function in intestinal epithelial cells. APMIS 119 (1), 49–56.
Foellmann, W., Behm, C., Degen, G.H., 2014. Toxicity of the mycotoxin citrinin and its metabolite dihydrocitrinone and of mixtures of citrinin and ochratoxin A *in vitro*. Arch. Toxicol. 88 (5), 1097–1107.
Fujiya, M., Musch, M.W., Nakagawa, Y., Hu, S., Alverdy, J., Kohgo, Y., Schneewind, O., Jabri, B., Chang, E.B., 2007. The *Bacillus subtilis* quorum-sensing molecule CSF contributes to intestinal Homeostasis via OCTN2, a host cell membrane transporter. Cell Host Microbe 1 (4), 299–308.
Gan, F., Hu, Z., Zhou, Y., Huang, K., 2017. Overexpression and low expression of selenoprotein S impact ochratoxin a-induced porcine cytotoxicity and apoptosis *in vitro*. J. Agric. Food Chem. 65 (32), 6972–6981.
Gao, Y., Li, S., Wang, J., Luo, C., Zhao, S., Zheng, N., 2018. Modulation of intestinal epithelial permeability in differentiated Caco-2 cells exposed to aflatoxin m1 and ochratoxin A individually or collectively. Toxins 10 (1), 13.
Gratz, S., Wu, Q.K., El-Nezami, H., Juvonen, R.O., Mykkanen, H., Turner, P.C., 2007. *Lactobacillus rhamnosus* strain GG reduces aflatoxin B-1 transport, metabolism, and toxicity in Caco-2 cells. Appl. Environ. Microbiol. 73 (12), 3958–3964.
Gu, M.J., Song, S.K., Park, S.M., Lee, I.K., Yun, C.-H., 2014. *Bacillus subtilis* protects porcine intestinal barrier from deoxynivalenol via improved zonula occludens-1 expression. Asian-Australas. J. Anim. Sci. 27 (4), 580–586.
Hubatsch, I., Ragnarsson, E.G., Artursson, P., 2007. Determination of drug permeability and prediction of drug absorption in Caco-2 monolayers. Nat. Protoc. 2 (9), 2111–2119.
Khalil, A.A., Abou-Gabal, A.E., Abdellatef, A.A., Khalid, A.E., 2015. Protective role of probiotic lactic acid bacteria against dietary fumonisin B1-induced toxicity and DNA-fragmentation in sprague-dawley rats. Prep. Biochem. Biotechnol. 45 (6), 530–550.
Kumar, R., Ansari, K.M., Chaudhari, B.P., Dhawan, A., Dwivedi, P.D., Jain, S.K., Das, M., 2012. Topical application of ochratoxin A causes DNA damage and tumor initiation in mouse skin. PLoS One 7 (10), e47280.
Kuo, I.H., Carpenter-Mendini, A., Yoshida, T., McGirt, L.Y., Ivanov, A.I., Barnes, K.C., Gallo, R.L., Borkowski, A.W., Yamasaki, K., Leung, D.Y., Georas, S.N., De Benedetto, A., Beck, L.A., 2013. Activation of epidermal toll-like receptor 2 enhances tight junction function: implications for atopic dermatitis and skin barrier repair. J. Invest. Dermatol. 133 (4), 988–998.
Liu, J., Wu, S., Shen, H., Cui, J., Wang, Y., Xing, L., Wang, J., Yan, X., Zhang, X., 2015. Ochratoxin A induces DNA damage and G2 phase arrest in human esophageal epithelium Het-1A cells *in vitro*. J. Toxicol. Sci. 40 (5), 657–665.
Lodemann, U., 2010. Effects of Probiotics on Intestinal Transport and Epithelial Barrier Function. Bioactive Foods in Promoting Health: Probiotics and Prebiotics. Elsevier Inc., pp. 303–333.
Malir, F., Ostry, V., Pfohl-Leszkowicz, A., Malir, J., Toman, J., 2016. Ochratoxin A: 50 years of research. Toxins 8, 191.
Pozarowski, P., Darzynkiewicz, Z., 2004. Analysis of cell cycle by flow cytometry. Methods Mol. Biol. NJ 281, 301–311 Humana Press Inc., Totowa.
Ramyaa, P., Padma, V.V., 2013. Ochratoxin-induced toxicity, oxidative stress and apoptosis ameliorated by quercetin - modulation by Nrf2. Food Chem. Toxicol. 62, 205–216.
Romero, A., Ares, I., Ramos, E., Castellano, V., Martinez, M., Martinez-Larranaga, M.-R., Anadon, A., Martinez, M.-A., 2016. Mycotoxins modify the barrier function of Caco-2 cells through differential gene expression of specific claudin isoforms: protective effect of illite mineral clay. Toxicology 353, 21–33.
Shi, L., Liang, Z., Li, J., Hao, J., Xu, Y., Huang, K., Tian, J., He, X., Xu, W., 2014. Ochratoxin A biocontrol and biodegradation by *Bacillus subtilis* CW 14. J. Sci. Food Agric. 94 (9), 1879–1885.
Suzuki, T., 2013. Regulation of intestinal epithelial permeability by tight junctions. Cell. Mol. Life Sci. 70 (4), 631–659.
Teitelbaum, J.E., Walker, W.A., 2002. Nutritional impact of pre- and probiotics as protective gastrointestinal organisms. Annu. Rev. Nutr. 22, 107–138.
Tominaga, H., Ishiyama, M., Ohseto, F., Sasamoto, K., Hamamoto, T., Suzuki, K., Watanabe, M., 1999. A water-soluble tetrazolium salt useful for colorimetric cell viability assay. Anal. Commun. 36, 47–50.
Vermes, I., Haanen, C., Steffens-Nakken, H., Reutelingsperger, C., 1995. A novel assay for apoptosis flow cytometric detection of phosphatidylserine expression on early apoptotic cells using fluorescein labelled Annexin V. J. Immunol. Methods 184 (1), 39–51.
Wan, L.Y., Chen, Z.J., Shah, N.P., El-Nezami, H., 2016a. Modulation of intestinal epithelial defense responses by probiotic bacteria. Crit. Rev. Food Sci. Nutr. 56 (16), 2628–2641.
Wan, M.L.Y., Turner, P.C., Allen, K.J., El-Nezami, H., 2016b. *Lactobacillus rhamnosus* GG modulates intestinal mucosal barrier and inflammation in mice following combined dietary exposure to deoxynivalenol and zearalenone. J. Funct. Foods 22, 34–43.
Wang, Y., Wang, L., Liu, F., Wang, Q., Selvaraj, J.N., Xing, F., Zhao, Y., Liu, Y., 2016. Ochratoxin A producing fungi, biosynthetic pathway and regulatory mechanisms. Toxins 8, 83.
Yanagihara, S., Fukuda, S., Ohno, H., Yamamoto, N., 2012. Exposure to probiotic *Lactobacillus* acidophilus l-92 modulates gene expression profiles of epithelial Caco-2 cells. J. Med. Food 15 (6), 511–519.
Yang, B., Lv, Y., Chen, Y., Wang, J., Tang, W., Guo, S., 2008. Inhibitory action of soybean beta-conglycinin hydrolysates on Salmonella typhimurium translocation in Caco-2 epithelial cell monolayers. J. Agric. Food Chem. 56 (16), 7522–7527.
Yang, Q., He, X., Li, X., Xu, W., Luo, Y., Yang, X., Wang, Y., Li, Y., Huang, K., 2014. DNA damage and S phase arrest induced by ochratoxin A in human embryonic kidney cells (HEK 293). Mutat. Res. 765, 22–31.
Ye, X., Li, P., Yu, Q., Yang, Q., 2013. *Bacillus subtilis* inhibition of enterotoxic *Escherichia coli*-induced activation of MAPK signaling pathways in Caco-2 cells. Ann. Microbiol. 63 (2), 577–581.
Zhou, Y., Gan, F., Hou, L., Zhou, X., Ibrahim, Y.A.A., Huang, K., 2017. Modulations of DNMT1 and HDAC1 are involved in the OTA-induced cytotoxicity and apoptosis *in vitro*. Chem. Biol. Interact. 278, 170–178.
Zhu, L., Zhang, B., Dai, Y., Li, H., Xu, W., 2017. A review: epigenetic mechanism in ochratoxin A toxicity studies. Toxins 9, 113.